Multifunctional "Dy(hfa)$_3$•glyme" adducts: synthesis and magnetic/luminescent behaviour

Anna L. Pellegrino,[a] Claudia Mezzalira,[b] Francesco Mazzer,[b] Lila Cadi-Tazi[c,†] Andrea Caneschi,[d] Dante Gatteschi,[c] Ignazio L. Fragalà,[a] Adolfo Speghini,[b,*] Lorenzo Sorace,[c,*] Graziella Malandrino[a,*]

[a]Dipartimento Scienze Chimiche, Università degli Studi di Catania, and INSTM UdR Catania, Catania, 95125, Italy

[b] Department of Biotechnology, University of Verona and INSTM UdR Verona, Strada Le Grazie 15, I-37134 Verona, Italy

[c]Department of Chemistry "U. Schiff", University of Florence and INSTM UdR Firenze, Sesto Fiorentino (FI) 50019, Italy

[d]Department of Industrial Engineering -DIEF, University of Florence and INSTM UdR Firenze, Via di S. Marta, 3 - 50139 Firenze (FI), Italy

[†] Current address: Département de Chimie École Normale Supérieure Paris-Saclay

Abstract

Dysprosium β-diketonate compounds have recently gained a lot of attention due to their intriguing multifunctional properties. In this paper, a series of "Dy(hfa)$_3$·glyme" adducts have been prepared through a one-pot reaction, in dichloromethane, from dysprosium (III) acetate monohydrate, hexafluoroacetylacetone and glyme [Hhfa = 1,1,1,5,5,5-hexafluoroacetylacetone, glyme = bis-(2-methoxyethyl)ether, 2,5,8,11-tetraoxadodecane, 2,5,8,11,14-pentaoxapentadecane]. Based on the length of the polyether, various coordination frameworks have been obtained going from a mononuclear Dy(hfa)$_3$•diglyme adduct, to a polymeric chain system for the Dy(hfa)$_3$•2H$_2$O•triglyme and an ionic structure for the [Dy(hfa)$_2$•tetraglyme]$^+$[Dy(hfa)$_4$]$^-$. The relationship between the coordination framework in the "Dy(hfa)$_3$glyme" series and the magnetic and luminescent properties has been deeply investigated.

Introduction

In recent years, the synthesis and characterization of molecular complexes simultaneously exhibiting interesting optical and magnetic properties has significantly increased [1–4].

In particular, the most investigated and interesting systems in this field are those containing lanthanide ions (Ln) which can show both single-molecule magnets (SMMs) behavior and photoluminescence, owing to their peculiar electronic structures [5–7].

Single-molecule magnets behavior is the ability of a molecular complex to retain its magnetization, in the absence of long-range order, for a long time at a given temperature due to the presence of a magnetic anisotropy barrier [8,9]. This results in magnetic bistability at low temperature making these systems of interest in perspective applications as high density magnetic memory units, molecular qubits and in molecular spintronics [10–14]. Lanthanide based complexes have first been shown to behave as SMMs single-ion magnets (SIMs) by Ishikawa et al. in 2003, who investigated a phthalocyaninato lanthanide complex with a "double-decker" structure of the general formula $[LnPc_2]^-$ [15]. Since then, an incredible amount of research has been performed on Ln-SMMs based on organic coordinating network of phtalocyanine [16,17], polyoxometalate [18–20], macrocyclic Schiff base ligands [21–26], radicals [27], and more recently organometallic complexes [28], holding the record for the highest magnetization blocking temperature [29,30].

β-Diketonates [31–33], have also been exploited since the beginning of the study on Ln-SMM as anionic ligands. $[Dy(acac)_3(H_2O)_2]$ (acac = acetilacetonate) is among the first single-ion lanthanide complexes to have been reported to show slow relaxation of the magnetization, which has been the subject of detailed experimental and theoretical studies [31,34]. Following this seminal example, various groups have reported simple β-diketonate complexes adducted with a Lewis base showing either SMM behaviour [35–38] or so-called Single Chain Magnet behaviour [39], where the reversal of the magnetization occurs by following Glauber dynamics.

In most of the cases reported up to now, in β-diketonates dysprosium metal ion exhibits Ising-type ground states with a local symmetry of D_{4d} such as in the $[Dy(acac)_3(H_2O)_2]$ and $[Dy(acac)_3(phen)]$

(phen = phenanthroline) [31,36]. The complexes [Dy(dpq)(acac)$_3$] and [Dy(dppz)(acac)$_3$], obtained using large aromatic derivatives as co-ligands, show a significant enhancement of the anisotropy barrier compared with previous adducts [40]. Although the majority of these SIMs contain 4f-centers with close to D_{4d} axial ligand-field symmetry, coordination spheres of lower symmetry are also observed [26,41].

At the same time β-diketonates derivatives of some lanthanide ions are known for being highly luminescent [42,43]. It is well known that the lanthanides emission is due to transitions inside the partially filled 4f shell. Since the 4f shell is shielded by the $5s^2 5p^6$ shell, the electronic configuration of trivalent lanthanide ions is only barely perturbed by ligands in the first and second coordination sphere. This shielding is responsible for the narrow-band emission and long lifetimes of excited states of these materials. Therefore, if on one hand the luminescence emission by lanthanides is an efficient process, on the other hand the light absorption is very weak. For this reason, a phenomenon known as "antenna-effect" is desirable: Weissman [44] discovered that organic chromophores, due to their intense absorption bands, can transfer their absorbed energy to the lanthanide ions by intramolecular energy transfer. The commonly accepted mechanism of this process is the one described by Crosby and Whan [45]. It consists of the excitation of the organic ligand and the energy transfer between its lowest triplet level and the accepting level of the lanthanide ion. In order to have an efficient energy transfer between ligand and Ln(III), the ligand triplet state should be at least 2000 cm^{-1} higher in energy than the lanthanide ion emitting state [46]. Since the energy differences between triplet states of hfa and phen and the emitting level of Dy(III) is higher than this value, an efficient energy transfer occurs and the luminescence properties of these materials are improved. Furthermore, the phen is an ancillary ligand that enhance the rigidity of the complex, reducing non-radiative relaxation processes and then improving the luminescence efficiency [44].

In this perspective, the present work reports on various dysprosium β-diketonate polyether adducts of general formula "Dy(hfa)3•glyme" [Hhfa = (1,1,1,5,5,5-hexafluoroacetylacetone); glyme = diglyme (bis(2-methoxyethyl)ether), triglyme (2,5,8,11-tetraoxadodecane), and tetraglyme

(2,5,8,11,14-pentaoxapentadecane)] from their syntheses to related magnetic and luminescence studies. The effect of polyether length on the coordination sphere of the Dy ion has been correlated to the observed magnetic and luminescent properties.

Experimental Section

Reagents. Commercial dysprosium acetate monohydrate and Hhfa were purchased from STREM Chemicals Inc, while diglyme, triglyme and tetraglyme were purchased from Sigma-Aldrich. All chemicals were used without any further purification.

General procedures. The reactions were conducted under normal laboratory conditions. Infrared transmittance spectra were recorded using a Jasco FT/IR-430 spectrometer as nujol mulls between NaCl plates in the 4000-400 cm^{-1} range. The instrumental resolution was 2 cm^{-1}. The melting points were measured in air with a Koeffler microscope. Thermogravimetric analyses (TGA) were performed using a Mettler Toledo TGA/SDTA 851^{e} under prepurified nitrogen flow fed into the working chamber at 30 sccm, with a 5°C/min heating rate at atmospheric pressure. Differential scanning calorimetry (DSC) were carried out using a Mettler Toledo Star System DSC 3 with a heating rate of 5 °C/ min from 25 °C up to 400 °C under prepurified nitrogen. Weights of the samples were between 6-14 mg.

Optical spectroscopy

The excitation spectra of the powder samples were acquired using a Nanolog/Fluorolog-3, spectrofluorometer, equipped with a xenon lamp (450 W) and a R928 (Hamamtsu) photomultiplier. The experiment has been conducted in a face-front geometry at 22.5° and the spectra were collected with an optical spectral resolution of 0.5 nm. Emission spectra were measured using a 450 nm diode laser as an excitation source, Czerny-Turner monochromator (Andor, Shamrock 500i) equipped with a 1200 lines/mm grating (estimated spectral resolution 0.12 nm) and an iDus CCD camera cooled at -80 °C. The emission signal was collected with a 40x microscopy objective (Nikon, Plan Fluor) using a beamsplitter mirror 30:70=R:T (Thorlabs, UV-Fused Silica substrate, 400-700 nm).

Synthesis of Dy(hfa)$_3$•diglyme (Dy-1). 1.7304 g (5.0954 mmol) of Dy($CH_3COO)_3$·H_2O was first suspended in dichloromethane. Diglyme 0.69 ml (4.8 mmol; d=0.940 g/ml) was added to the suspension. H-hfa 2.04 ml (14.4 mmol; d=1.47 g/ml) was added to it under vigorous stirring after 10 minutes and the mixture was refluxed under stirring for 1 h. The pale yellow solution was collected by filtration in air and the excess of Dy($CH_3COO)_3$·H_2O was filtered off. The pale yellow product was obtained upon evaporation of the solvent. It was washed two to three times in pentane. The reaction yield was 87%. The melting point of the crude product was 66-69°C/760 Torr.

Synthesis of Dy(hfa)$_3$•2H_2O•triglyme (Dy-2). Prepared using a procedure analogous to that described for the adduct **1** from 1.6576 g (4.8810 mmol) of Dy($CH_3COO)_3$·H_2O, 0.87 ml (4.8 mmol; d=0.986 g/ml) of triglyme and 2.04 ml (14.4 mmol) of H-hfa. Yield 91%. The melting point of the crude yellowish product was 60-77 °C/760 Torr.

Synthesis of [Dy(hfa)$_2$•tetraglyme]$^+$[Dy(hfa)$_4$]$^-$ (Dy-3). Prepared using a procedure analogous to that described for the precedent adducts from 1.7427 g (5.1316 mmol) of Dy($CH_3COO)_3$·H_2O, 0.53 ml (4.8 mmol; d=1.0132 g/ml) of tetraglyme and 2.04 ml (14.4 mmol) of H-hfa. The solid product was filtered off. The product was a mixture of the excess of Dy($CH_3COO)_3$·H_2O and of [Dy(hfa)$_2$•tetraglyme]$^+$[Dy(hfa)$_4$]$^-$. The product **3** was isolated by dissolving the mixture in acetone, since **3** is soluble in acetone, while, the Dy acetate is not soluble in the same solvent. The pale yellow adduct **3** was recovered by acetone evaporation. Yield 72%. The compound melts at 186-191 °C/760 Torr.

Magnetic characterization

Temperature-dependent direct current (DC) magnetic measurements were conducted on a Quantum Design MPMS SQUID magnetometer. Raw data were treated for the underlying sample holder contribution and corrected for the intrinsic diamagnetism of the sample using Pascal's constants.[47] AC magnetic susceptibility measurements were carried out on both the aforementioned SQUID and a Quantum Design PPMS in AC mode at both zero and applied external DC field in the presence of

a 5 Oe oscillating magnetic field. The latter set-up was used for frequencies between 10 Hz and 10 kHz, whereas the former was used for frequencies in the range 0.1 Hz-1 kHz. Powders were pressed in a pellet to avoid field-induced orientation of the crystallites.

Description of the code for fit of ac susceptibility data

The fits of the ac susceptibility data using generalized Debye model were obtained with the help of a home-developed code described hereafter. The curve fitting was performed with the *lsqnonlin* nonlinear least-squares solver available in Matlab's optimization toolbox [48].

Generalized Debye model was coded as a parametric function of x where $x = [\chi_S, \chi_T, \alpha, \tau]$ are the parameters introduced in the Debye model. The algorithm then simultaneously optimizes the residual values of $\chi'_{fit}(x)$ - $\chi'_{data}(x)$ and $\chi''_{fit}(x)$ - $\chi''_{data}(x)$. As χ'' data usually gives more precise results on the fit parameters (because they show relevant maximum), the optimization of x is carried out with default values of 80% weight on the χ'' residual and 20% for χ'. Additionally, Tikhonov regularization of parameters with norm l_2 is added to the optimized function to avoid aberrant values of the parameters. The default Lagrange parameter is chosen as λ=0.001.

The optimization is then carried out on x by optimizing the expression in equation \ref{min} using the Trust-Region-Reflective Least Squares algorithm [49].

$$\min_x \left\{ \left[0.2 \times \left(\chi'_{fit} - \chi'_{data} \right) \right]^2 + \left[0.8 \times \left(\chi''_{fit} - \chi''_{data} \right) \right]^2 + \lambda^2 \sum x_i^2 \right\}$$

To obtain more trustable fits, a weight was beforehand applied to the data, based on the standard deviation given by the measuring instrument. By doing so, more trustable points (with lower standard deviations) carry more weight in the fit process.

As AC data usually show continuity (when the external dc field or temperature is monotonically scanned) each set of parameters is used as initial guess for the next curve's optimization process. Other initial guesses are also available in the program, corresponding to classical shapes of AC curves. To give an error estimation on each obtained parameter, the 95 % confidence intervals were

computed by inserting residuals and Jacobian matrices in matlab's nlparci function. However, more accurate errors could be calculated by taking into account the parameters distribution described in the generalized Debye model [50].

Ultimately, the program plots two figures with $\{\chi'_{fit}(x), \chi'_{data}(x)\}$ and $\{\chi''_{fit}(x), \chi''_{data}(x)\}$ against the AC frequency, at each temperature or DC field scanned. The fitted parameters are stored in a separated file for further processing.

Results and discussions

Synthesis. The "$Dy(hfa)_3 \bullet L$" adducts can be easily prepared through a single-step reaction from dysprosium acetate monohydrate, hexafluoroacetylacetone and polyether in dicloromethane following eq 1 or 2:

$$Dy(CH_3COO)_3 \bullet H_2O + 3H\text{-}hfa + L \rightarrow Dy(hfa)_3 \bullet L + 3\ CH_3COOH + H_2O \quad (L=diglyme) \quad (eq.1)$$

or

$$Dy(hfa)_3 \bullet (H_2O)_2 \bullet L \qquad (L=triglyme)$$

$$2Dy(CH_3COO)_3 \bullet H_2O + 6H\text{-}hfa + L \rightarrow [Dy(hfa)_2 \cdot L]^+ \bullet [Dy \cdot (hfa)_4]^- + 6\ CH_3COOH + H_2O$$

$$L = Tetraglyme \qquad (eq.2)$$

The synthetic strategy produces adducts with a high yield in a single step, thus representing a low-cost route from commercially available chemicals.

A slight excess of Dysprosium acetate monohydrate favors the isolation of the product since the excess remains insoluble and can be easily filtered off. The adducts are soluble in dichloromethane and acetone and less soluble in common organic solvents such as pentane, n-octane and n-decane.

The present synthetic procedure gives rise to non-hygroscopic and water-free adducts **Dy-1** and **Dy-**

3, while H_2O molecules have been found coordinated to the Dy center in **Dy-2** (*vide infra*).

Infrared spectra. The IR spectra of the "Dy(hfa)$_3$•glyme" adducts, reported in figure 1, confirm the formation of the complexes. In fact, all the spectra show two characteristic peaks around 1650 and 1560 cm^{-1} associated with the C=O and C=C stretching frequencies that substantiate the coordination of the hfa ligand to the metal. The absence of any bands around 3600-3400 cm^{-1} in the spectra of **Dy-1** and **Dy-3** is indicative of H_2O-free species. By contrast, the broad envelope with two bands at 3361 and 3268 cm^{-1} in the spectrum of **Dy-2** is associated with water coordination. The region between 800 and 1100 cm^{-1} may be considered as fingerprints of the glyme coordination to the dysprosium hexafluoroacetylacetonate moiety.

It is worthy to compare the numbers and positions of peaks in this region with those found for the yttrium analogous adducts. In Table 1 the stretching of the polyether C-O in Dy adducts is compared with the analogous Y ones [51]. The similar IR spectra in this region point to similar coordination environments for the Y and Dy ions in the two series of complexes. This observation finds counterpart in the comparable ionic radii, reported for an height coordination, of Dy^{3+} (r = 1.027 Å) and Y^{3+} (r = 1.019 Å) [52].

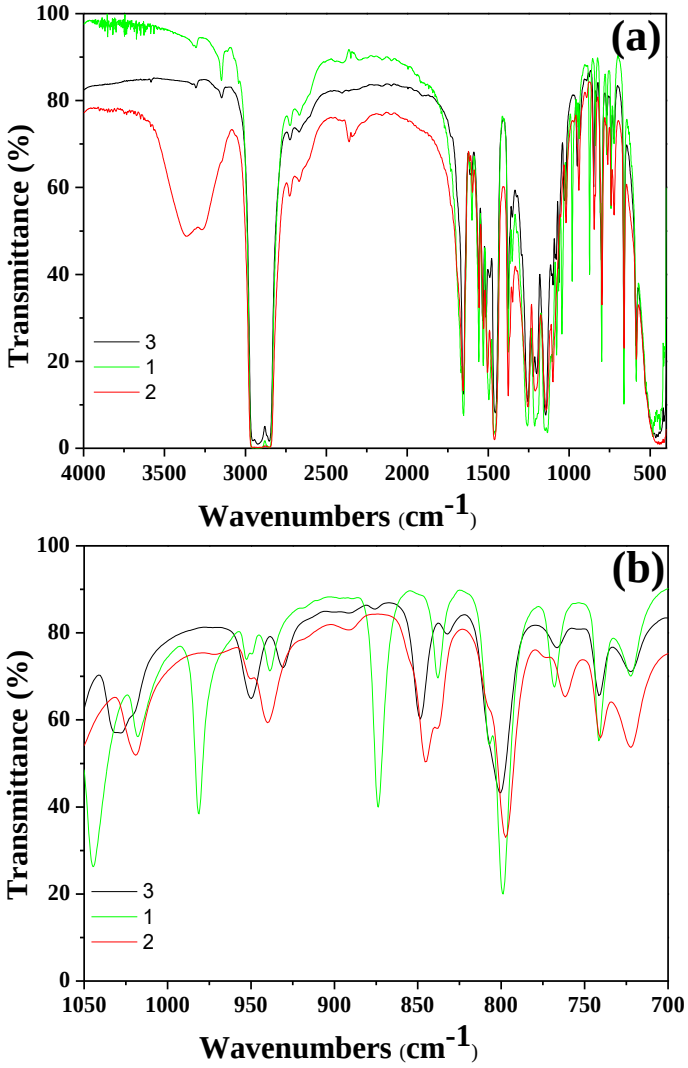

Fig. 1. FT-IR spectra (nujol mulls) of (a) the "Dy(hfa)$_3$•glyme" adducts and (b) a magnification of the fingerprint region (700-1050 cm^{-1}) for glyme coordination.

Table 1. Vibration modes of "Dy(hfa)$_3$•glyme" with diglyme, triglyme and tetraglyme.

"M(hfa)$_3$•glyme"	**diglyme C-O stretching (cm^{-1})**	**triglyme C-O stretching (cm^{-1})**	**tetraglyme C-O stretching (cm^{-1})**
Dy	837 (w), 873 (m), 981 (w), 1017 (m)	837 (vw), 844(m), 939(w), 1018 (m)	832(vw), 848(m), 930 (w), 950(m), 1028(m)
Y	835 (w), 870 (m), 950 (w), 1010 (m)	840(w), 940(w), 1020 (w)	830(vw), 850(m), 930(w), 950(m), 1035(m)

Thermal properties. The thermal behavior of the three complexes has been investigated through thermogravimetric analyses (TG) and differential scanning calorimetry (DSC). The latter characterization has allowed to make a comparison with analogous rare-earth compounds of similar ionic radius, thus corroborating the isostructural nature of these complexes. Figure 2 reports the DSC analyses of the adducts. The DSC scan of complex **Dy-1** shows one endothermic peak at 67.8 °C due to melting of the adduct and matches the melting range (66-69 °C) observed with the Koeffler microscope. Evaporation occurs in the 220-270 °C temperature range.

The broad endothermic peak at 72.5 °C, observed for the compound **Dy-2**, can be mainly associated with the melting of the product. Nevertheless, it cannot be excluded that another kind of process, that is, a solid-phase transition peak, may be hidden under the same peak. An exothermic peak has been also found between 260 °C and 310 °C.

Finally adduct **Dy-3** shows a sharp endothermic peak at 189.6 °C associated with the melting process and a very broad peak in the range 210-310 °C, which accounts for evaporation. The very high melting point observed for **Dy-3** is similar to those observed for the Y, Eu, Gd, and Ho homologues [53].

In Table 2, the melting points of the diglyme, triglyme and tetraglyme adducts are reported for a series of small ionic radius rare-earth ions. For comparison, the melting points of the related adducts of Lanthanum are reported as well. It is interesting to observe that a larger ionic radius rare-earth ion, such as La^{3+} (r = 1.16 Å) gives rise to a mononuclear $La(hfa)_3$•glyme adducts whatever the glyme and that the $La(hfa)_3$•tetraglyme shows a much lower melting point of 87.6 °C [54].

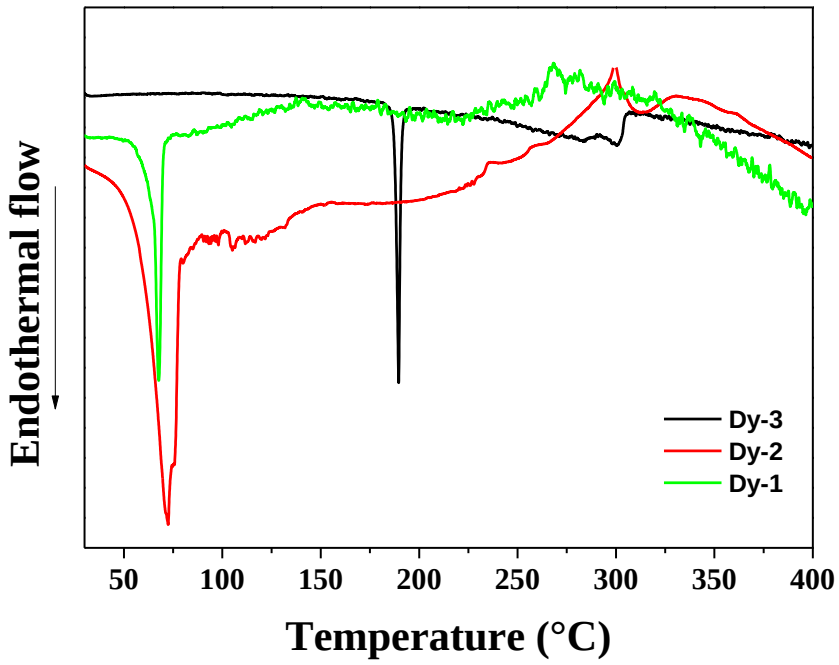

Fig. 2. DSC curves of the "Dy(hfa)$_3$•glyme" adducts in the 30-400 °C temperature range.

Table 2. Melting points of the diglyme, triglyme and tetraglyme adducts for a series of small ionic radius rare earth ions. The m.p of La adducts are reported for comparison.*

"M(hfa)$_3$•glyme"	**M(hfa)$_3$•diglyme phase transitions (C°)**	**M(hfa)$_3$•2H$_2$O•triglyme phase transitions (C°)**	**[M(hfa)$_4$]$^-$ [M(hfa)$_2$•tetraglyme]$^+$ phase transitions (C°)**
Dy	67.8 (m.)	72.5 (m.)	189.6 (m.)
Y (ref. [54])	62.2 (m.)	53.8 (m.)	176.9 (m.)
"M(hfa)$_3$•glyme"	**M(hfa)$_3$•diglyme m.p. (C°)**	**M(hfa)$_3$•triglyme m.p. (C°)**	**M(hfa)$_3$•tetraglyme m.p. (C°)**
La (ref. [53,55])	74.9 (m.)	79.3 (p.t.), 87.6 (p.t.), 145.8 (m.)	67(p.t.), 84 (m.)

*p.t. = solid-solid phase transition, m.= melting point.

Atmospheric pressure thermogravimetric analysis curves of "Dy(hfa)$_3$•L" and their related derivatives (DTG) are reported in Figure 3. The complex **Dy-1** shows an 89% weight loss in the 120-257 °C range and a 6% loss in the 257-450 °C range with a 5 % residue left at 400 °C. The broad DTG peak is centered at 248 °C.

The triglyme adduct **Dy-2** shows that the compound maintains a constant weight up to about 100 °C. This is the temperature at which the water molecules, coordinated to the Dy ion in accordance with IR and DSC data, are removed, indicating that **Dy-2** is a hydrated species. The observed weight loss of 3.2% compares well with the theoretical value (3.6%) found for the coordination of two water molecules to give the $Dy(hfa)_3 \bullet 2H_2O \bullet$triglyme complex. Vaporization process occurs in a higher temperature range, namely 125-250°C. Residue at 400 °C is about 5%.

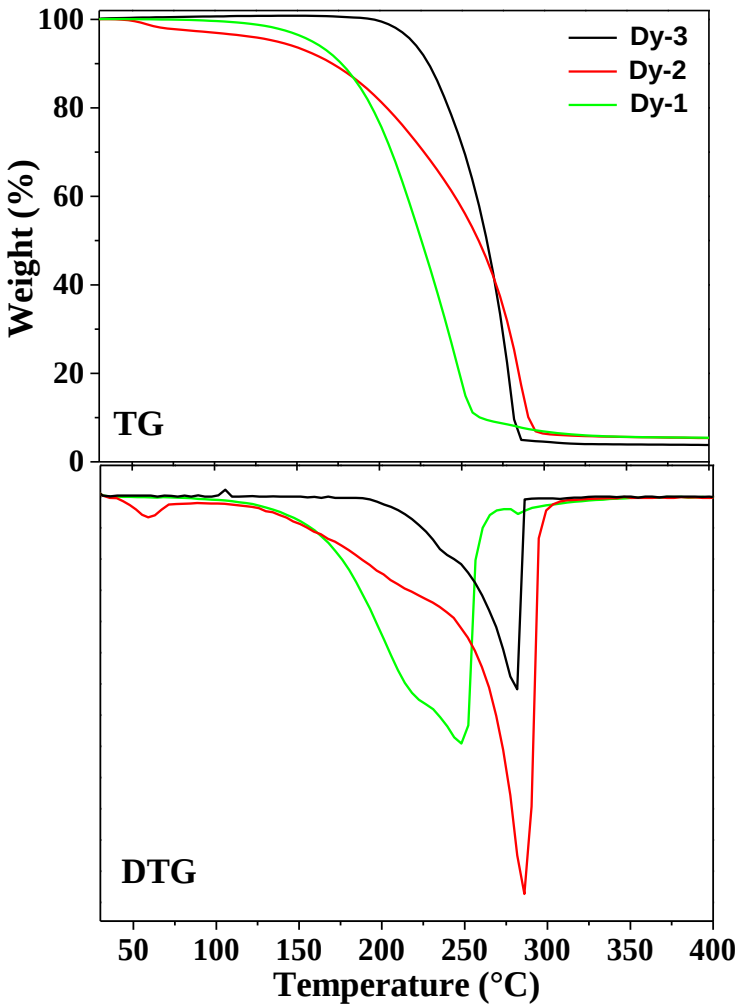

Fig. 3. TG-DTG curves of the "$Dy(hfa)_3$•glyme" adducts in the 30-400 °C temperature range.

A different behaviour has been observed for the tetraglyme complex **Dy-3**. In fact, it shows a lower volatility than the other adducts. The complex evaporates quantitatively in a single sublimation step in the 187-286 °C temperature range, with a residue of 3 % at 400 °C. Thus, the compound **Dy-3** is

thermally stable and the derivative curve of TG (DTG) consists of a single intense peak thus indicating that it evaporates quantitatively in the temperature range previously cited.

Thus, IR, TG and DSC data indicate that these adducts are isomorphous with complexes of rare-earth metals of small ionic radius. In particular, the adduct **Dy-1** is a monomeric molecule, the adduct **Dy-2** has a polymeric network with a formula of $M(hfa)_3 \bullet 2H_2O \bullet$triglyme and the **Dy-3** possesses an ionic structure of the type $[M(hfa)_4]^-[M(hfa)_2 \bullet$tetraglyme$]^+$.

The good thermal behaviour under atmospheric pressure of these adducts envisage excellent thermal properties for the deposition of these complexes as nanostructured films [56].

Magnetic characterization. The temperature dependence of χT for all the complexes is reported in Figure 4. The room temperature χT value per mole of Dysprosium(III) is close to the expected free-ion value ($^6H_{15/2}$, $g_J = 4/3$, $\chi T_{free\text{-}ion}$=14.02 emu K mol^{-1}) for all of them. On lowering temperature χT decreases due to progressive depopulation of excited sublevels of the J = 15/2 multiplet, split by the ligand field of the glyme. The observed difference in the thermal profile point to relevant differences in the coordination spheres of these complexes. The isothermal magnetization curves at low temperature (Inset of fig. 4, curves reported as M vs H/T) are on the contrary quite similar to each other, suggesting that the ground state doublet resulting from crystal field splitting has a similar composition in terms of m_J in the three derivatives. The observed saturation value in these curves is slightly above 5 μ_B (per mole of Dysprosium ion) for all the complexes, as almost invariably reported for Dysprosium(III) containing complexes, and in agreement with the expected effects due to Ligand Field splitting. The reduced magnetization curves measured at the three temperatures do not strictly superimpose on each other for any of the derivatives, thus suggesting that the ground state is not completely isolated from the excited ones.

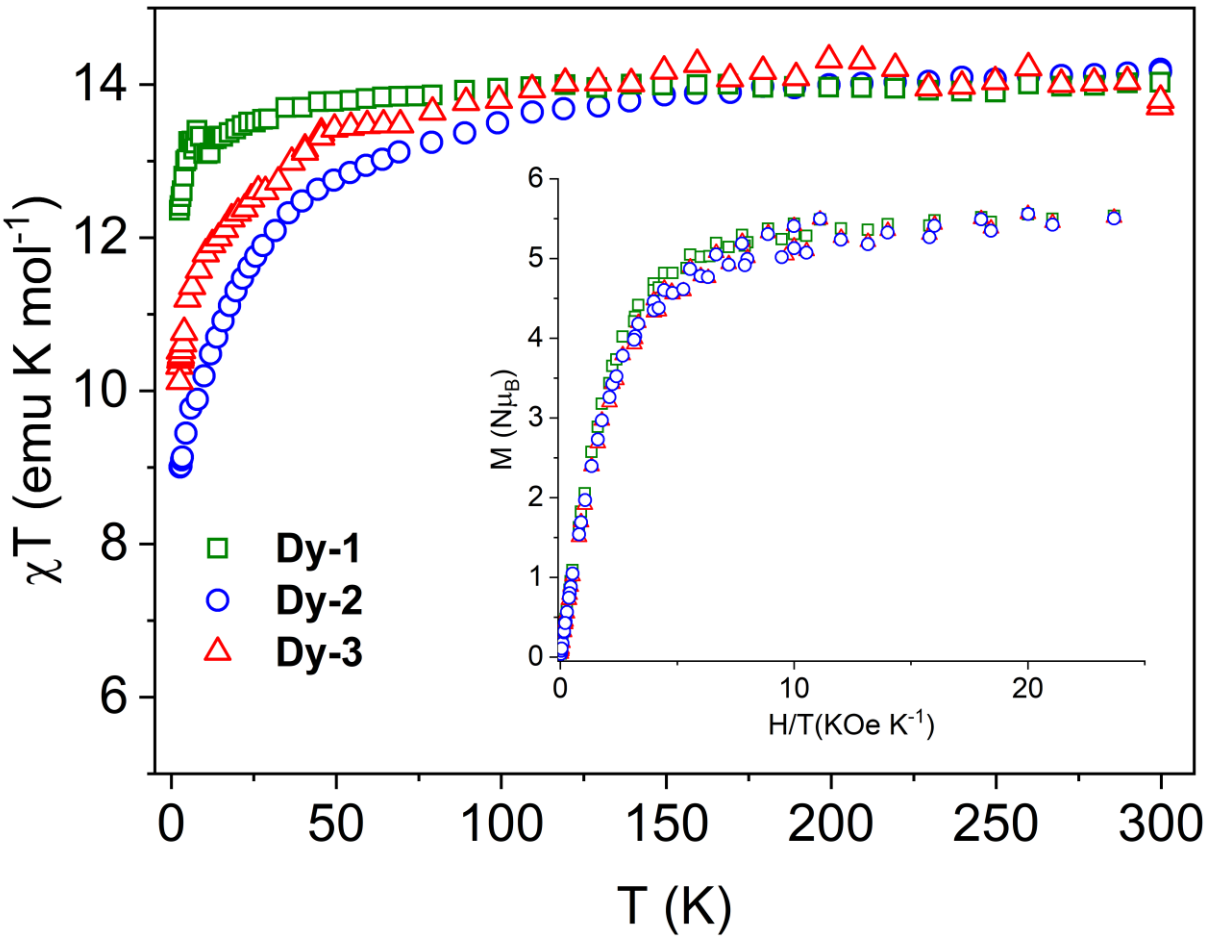

Fig. 4. χT vs T plot for the three complexes. (inset): Reduced Magnetization curves for the three derivatives measured at 1.9 2.5 and 5 K. Data are reported per mole of Dysprosium(III).

To probe magnetization relaxation processes in the three derivatives, AC susceptibility measurements were performed as a function of the external applied field (0-3 KOe), temperature (2-15 K), and frequency (0.02 Hz–10 kHz). Interestingly, all three samples show a non-zero value of the imaginary component of the susceptibility (χ'') in zero external applied field for frequencies above 1 KHz (Fig. 5). The position of the maximum is temperature independent up to 8 K and only weakly temperature dependent above, as long as it remains detectable in our setup. This suggests that this relaxation process is essentially due to QTM, possibly driven by the intermolecular dipolar interactions in the concentrated phase.

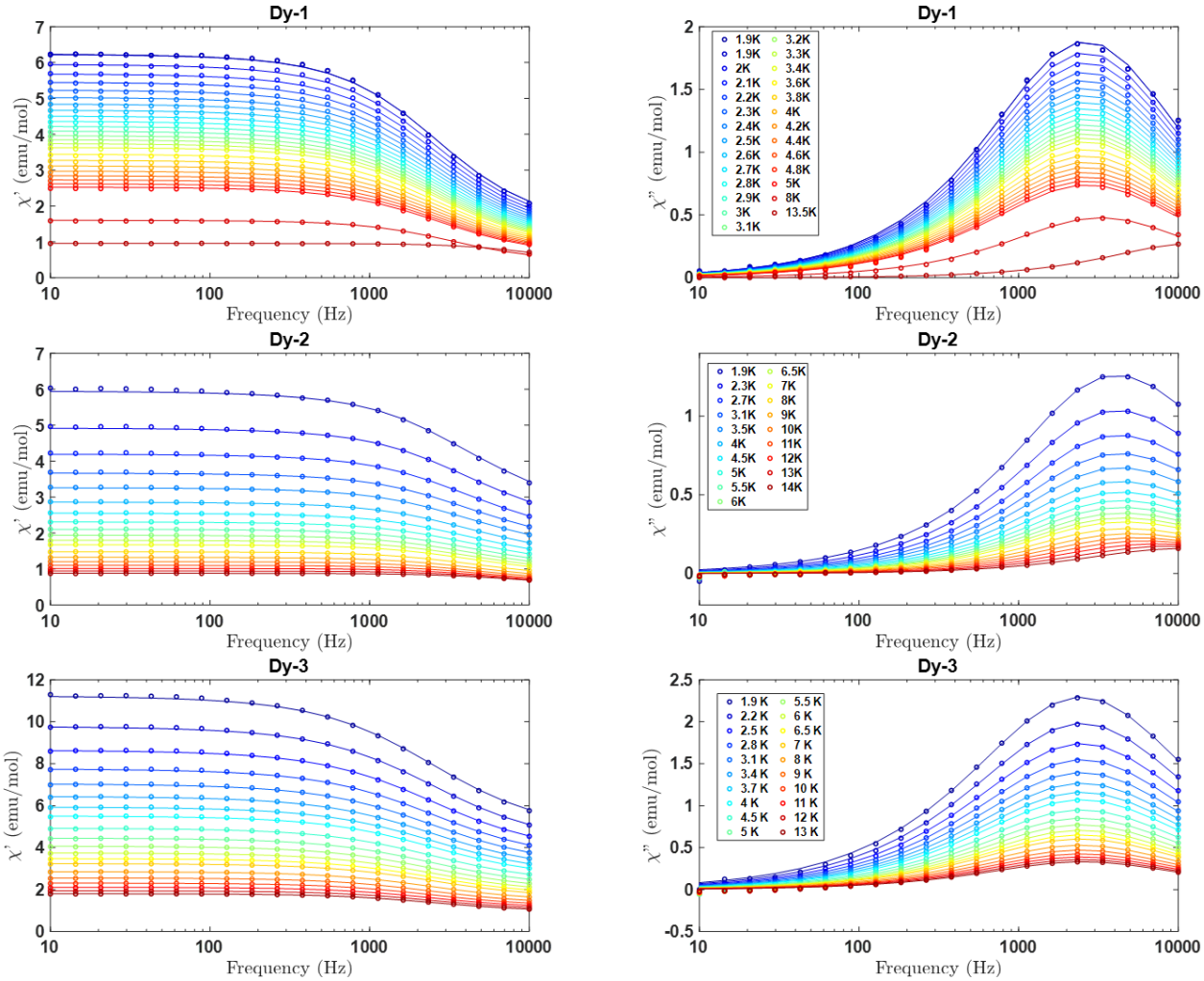

Fig. 5. Frequency dependence of the real (left) and the imaginary (right) component of the magnetic susceptibility for the three derivatives in zero applied field at different temperatures. The lines are the fit to the data using a generalized Debye model. Data are reported per mole of complex.

On applying an external dc field, this high frequency relaxation process is strongly suppressed while a much slower process starts to arise, visible as a low frequency tail (Fig. 6). This behavior is quite common in undiluted Dysprosium(III) containing complexes of axial symmetry [31,57,58].

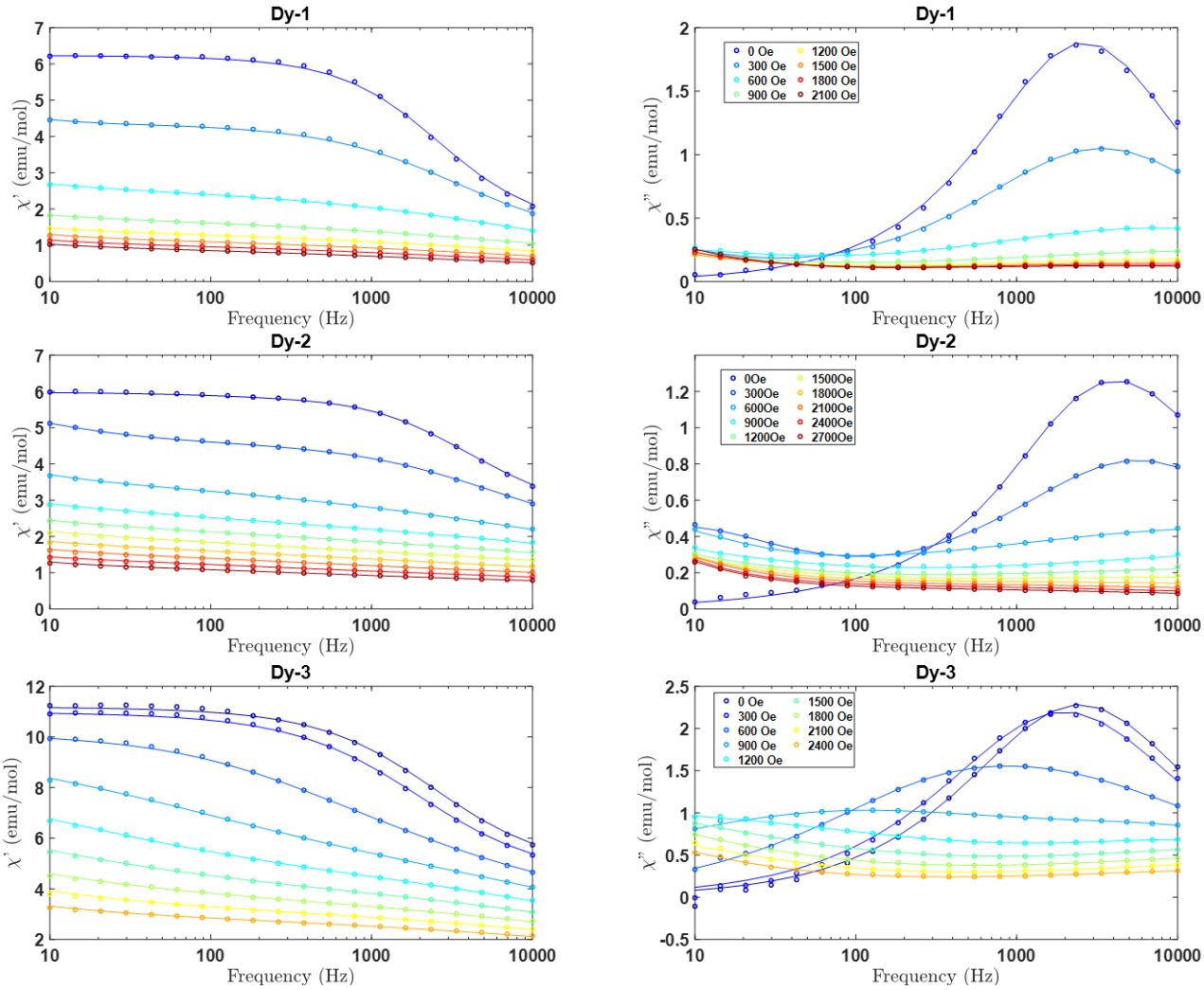

Fig. 6 Frequency dependence of the real (left) and imaginary (right) component of the magnetic susceptibility for the three derivatives at 1.9 K as a function of the external magnetic field. The lines are the fit to the data using a generalized Debye model assuming two contributions with field-dependent weights. Data are reported per mole of complex.

The temperature dependence of the dynamic magnetic susceptibility was then measured in an applied field of 2100 Oe, chosen as the optimum one for the three derivatives, down to 0.05 Hz and the corresponding curves fit by using a generalized Debye model (Fig. 7). It is worth noting that for all the complexes at low temperature the fast process at high frequency is not completely quenched, as evident by the non-zero value of χ'' at 10 KHz for all the three derivatives. This forced us to consider two different contributions to reproduce the data: however, only the parameters pertaining to the slowest process have a physical meaning. In this interpretation, the fastest one has to be considered

as a residue of the QTM dominating in zero-field. It is then interesting to notice that for **Dy-3**, which contains two different magnetic sites, only a single process is observed, suggesting that only one of the two centers is slowly relaxing. This is also consistent with the χ''/χ' ratio, which is approximately one half than for the other two derivatives.

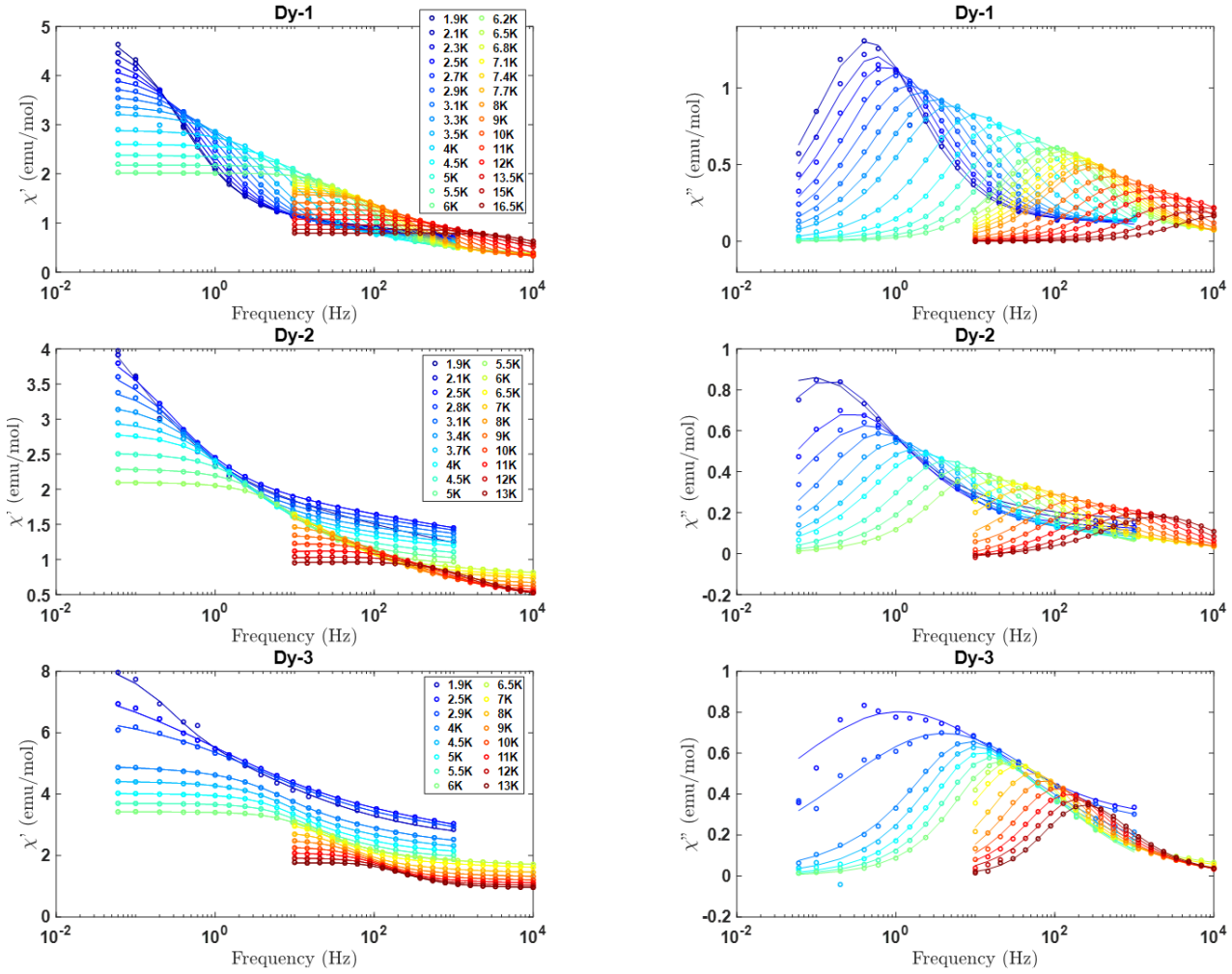

Fig. 7. Frequency dependence of the real (top) and imaginary (bottom) component of the magnetic susceptibility for the three derivatives in an external field of 2.1 KOe as a function of the temperature. The lines are the fit to the data using a generalized Debye model assuming two different contributions. Data are reported per mole of complex.

The extracted temperature dependence of the relaxation time of the slow process is reported in Fig. 8 for **Dy-1, Dy-2** and **Dy-3** as a log-log plot. In the absence of an applied field all the derivatives show similar QTM times, around 5 x 10^{-6} s.

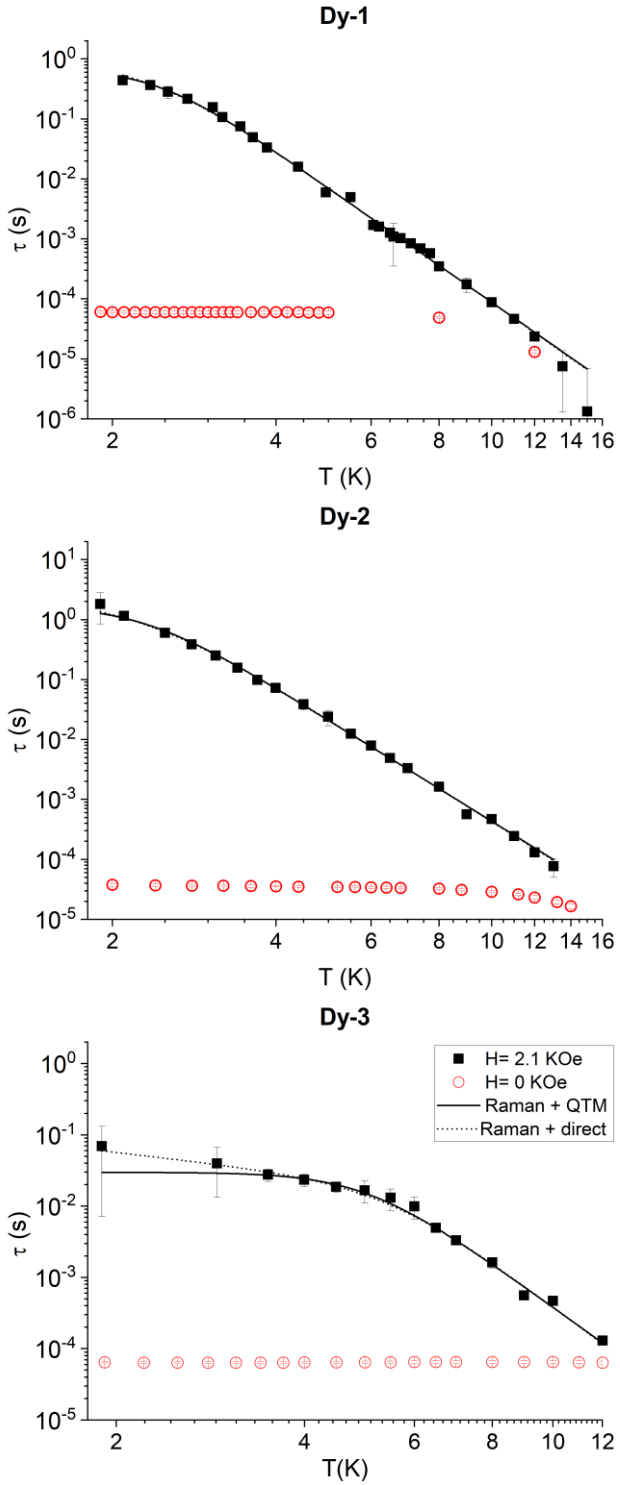

Fig. 8. Temperature dependence of the relaxation time for the three derivatives with and without external applied field and best fit curves obtained using the two models described in the text.

When considering the relaxation time under an applied field of 2.1 KOe, the linearity of the plot over a large range of temperature is evident for **Dy-1** and **Dy-2**, suggesting that in this temperature range

and with this applied field the Raman contribution to the relaxation is dominating.[59] Some curvature is still visible at low temperature: this might be either due to QTM being not completely quenched or to the contribution of a direct process. The low temperature deviation from pure Raman behaviour is particularly evident for **Dy-3.** We attribute this peculiar behaviour to the stronger dipolar interactions, which in this derivative involves the cationic and the anionic moieties. Based on the foregoing interpretation, we fitted the temperature dependence of the relaxation time as a function of temperature by two different equations, considering either a combined Raman/QTM relaxation, $\tau^{-1}=A_{Ram}T^{n} + B_{QTM}$ or a Raman/direct one, $\tau^{-1}=A_{Ram}T^{n} + C_{dir}T$, since the direct term, should in principle be present for the in-field data set. The obtained fits were of comparable quality, then not allowing discriminating between the two models. It is however to be stressed that for both models, the best-fit Raman exponent is for all the three derivatives close to 6 (see Table 3 for best fit parameters). This value, even if lower than the one theoretically expected [60], is in line with those reported for many different Lanthanide based molecular magnets. The non-observation of an Arrhenius-like behaviour suggest that the magnetic anisotropy barrier is high enough that this relaxation path only becomes accessible for these systems at higher temperatures. On the other hand, the efficiency of the Raman relaxation is likely to be related to the flexibility of the glyme ligand; interestingly a dominance of the Raman relaxation path has been reported also for crown-ether lanthanide complexes [58]. More detailed information on the relaxation processes in these complexes would require the obtainment and characterization of diamagnetically dilute isostructural analogues, which is beyond the scope of this paper.

Table 3. Best fit parameters for the two models describing the temperature dependence of the relaxation time.

	Raman + QTM			Raman + direct		
	A_{Ram} (s^{-1} K^{-n})	n	B_{QTM} (s^{-1})	A_{Ram} (s^{-1} K^{-n})	n	C_{dir}(s^{-1} K^{-1})
Dy-1	(5.5 ± 0.6) x10^{-3}	6.3 ± 0.07	1.4 ± 0.3	(4.8 ± 0.7)x10^{-3}	6.37 ± 0.08	0.6 ± 0.1
Dy-2	(5.7 ± 0.6) x10^{-3}	5.61 ± 0.06	0.6 ± 0.1	(4.8 ± 0.6) x 10^{-3}	5.69 ± 0.07	0.29 ± 0.04
Dy-3	(1.2 ± 0.5) x10^{-3}	6.3 ± 0.2	33 ± 4	(6 ± 3) x 10^{-4}	6.6 ±0.2	9. ± 1.

Luminescence properties.

The emission and excitation spectra of the adducts are presented in Figures 9 and 10, respectively.

The excitation spectra were recorded by monitoring the strongest emission at 573 nm. A broad band around 350 nm is assigned to the $S_0 \rightarrow S_1$ transition typical of the hfa ligand [61]. Other narrow excitation bands are related to 4f–4f transitions of Dy(III): $^6H_{15/2} \rightarrow {}^6P_{5/2}$, $^6H_{15/2} \rightarrow {}^4I_{13/2}$, $^6H_{15/2} \rightarrow {}^4G_{11/2}$, $^6H_{15/2} \rightarrow {}^4I_{15/2}$ and $^6H_{15/2} \rightarrow {}^4F_{9/2}$ were observed at 365 nm, 387 nm, 426 nm, 451 nm and 470 nm, respectively.

The emission spectra have been collected upon excitation at 450 nm, corresponding to the $^6H_{15/2} \rightarrow {}^4G_{11/2}$ transition of Dy(III). The emission spectra are dominated by a very strong band around 575 nm, in the yellow spectral region, due to the $^4F_{9/2} \rightarrow {}^6H_{13/2}$ transition of Dy(III). This electric-dipole transition is hypersensitive ($\Delta J=2$) and it strongly depends on the local environment around the lanthanide in the complexes. Since a slight variation of the band profile is observed for this band, the symmetry of the site where Dy(III) is accommodated is different [62]. A much weaker band around 660 nm with respect to the yellow emission, is observed, due to the $^4F_{9/2} \rightarrow {}^6H_{13/2}$ transition.

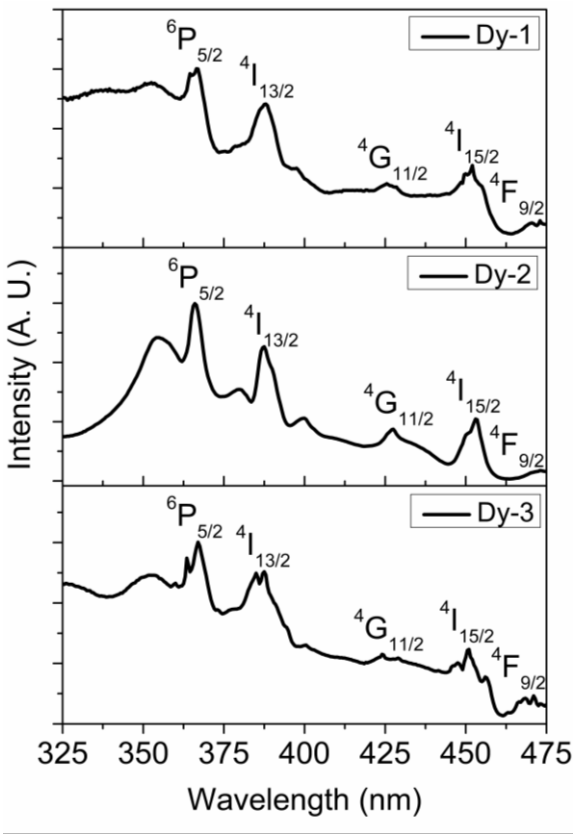

Fig. 9. Excitation spectra of the Dy(III) adducts (λ_{em}=573 nm). The labels refer to the excited levels populated by transitions starting from the $^6H_{15/2}$ ground state.

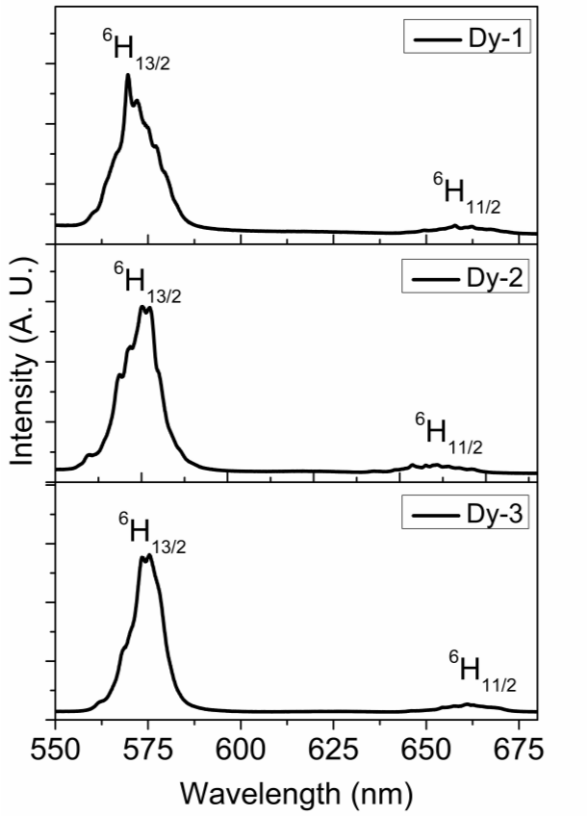

Fig. 10. Emission spectra of the Dy(III) adducts (λ_{em}=450 nm). The labels refer to the excited levels from which the radiative processes to the $^6H_{15/2}$ ground state take place.

Conclusions

The present one-pot synthetic strategy has proven an efficient route for the preparation of novel Dy adducts, that to our knowledge represent the first examples of lanthanide β-diketonate polyether adducts investigated regarding their multifunctional magnetic and luminescent properties. Both investigations point to a diverse behavior that can be related to differences in the Dy coordination sphere. The magnetic measurements indicate that all the three derivatives show slow magnetic relaxation in zero field, and a Raman dominant path is evident from the temperature dependence of the relaxation time measured in-field. In addition, all the samples show an interesting sharp yellow emission around 545 nm, that is more than 70% of the total emission in the visible range, upon excitation with radiation in the UV or -blue region. Finally, their thermal stability, as assessed through thermogravimetric measurements, suggests the possibility to apply these complexes for the fabrication of single monolayer systems through a molecular layer deposition approach.

Acknowledgments

A. L. P and G. M. acknowledge the University of Catania for financial support within the PIACERI research program UNICT 2020−22 Linea 2. A.S, C.M. and F.M. acknowledge University of Verona, Italy, for financial support in the framework of the “Joint Projects 2018”. Dr. Marco Giarola, of the Center of Technological Platforms, University of Verona, Italy, is gratefully acknowledged for technical support in the measurements of the optical spectroscopic properties. L. C.-T. acknowledges financial support from the Erasmus + program. L. S. acknowledges the financial support of MIUR, for the economic contribution within the "Progetto Dipartimenti di Eccellenza 2018-2022" allocated to Department of Chemistry "Ugo Schiff" (ref B96C1700020008).

References

[1] E. Cariati, R. Macchi, D. Roberto, R. Ugo, S. Galli, N. Casati, P. Macchi, A. Sironi, L. Bogani, A. Caneschi, D. Gatteschi, Polyfunctional inorganic-organic hybrid materials: an unusual kind of NLO active layered mixed metal oxalates with tunable magnetic properties

and very large second harmonic generation., J. Am. Chem. Soc. 129 (2007) 9410–20. https://doi.org/10.1021/ja0710712.
[2] M. Perfetti, F. Pointillart, O. Cador, L. Sorace, L. Ouhab, Luminescent Molecular Magnets, Mol. Magn. Mater. Concepts Appl. (2016) 1–5.
[3] M. Atzori, F. Artizzu, Functional Molecular Materials, Jenny Stanford Publishing, Boca Raton, 2016.
[4] L. Ouahab, ed., Multifunctional Molecular Materials, Jenny Stanford Publishing, New York, 2012.
[5] F. Pointillart, O. Cador, B. Le Guennic, L. Ouahab, Uncommon lanthanide ions in purely 4f Single Molecule Magnets, Coord. Chem. Rev. 346 (2017) 150–175. https://doi.org/10.1016/J.CCR.2016.12.017.
[6] J. Long, Y. Guari, R.A.S. Ferreira, L.D. Carlos, J. Larionova, Recent advances in luminescent lanthanide based Single-Molecule Magnets, Coord. Chem. Rev. 363 (2018) 57–70. https://doi.org/10.1016/J.CCR.2018.02.019.
[7] R. Marin, G. Brunet, M. Murugesu, Shining New Light on Multifunctional Lanthanide Single-Molecule Magnets, Angew. Chemie Int. Ed. 60 (2021) 1728–1746. https://doi.org/10.1002/ANIE.201910299.
[8] G. Christou, D. Gatteschi, D.N. Hendrickson, R. Sessoli, Single-Molecule Magnets, (2000) 66–71.
[9] A. Caneschi, D. Gatteschi, R. Sessoli, A.L. Barra, L.C. Brunel, M. Guillot, Alternating current susceptibility, high field magnetization, and millimeter band EPR evidence for a ground S = 10 state in $[Mn_{12}O_{12}(CH_3COO)_{16}(H_2O)_4].2CH_3COOH.4H_2O$, J. Am. Chem. Soc. 113 (1991) 5873–5874. https://doi.org/10.1021/ja00015a057.
[10] M.N. Leuenberger, D. Loss, Quantum computing in molecular magnets., Nature. 410 (2001) 789–93. https://doi.org/10.1038/35071024.
[11] D. Gatteschi, R. Sessoli, J. Villain, Molecular Nanomagnets, Oxford University Press, Oxford, UK, 2007. https://doi.org/10.1093/acprof:oso/9780198567530.001.0001.
[12] L. Bogani, W. Wernsdorfer, Molecular spintronics using single-molecule magnets., Nat. Mater. 7 (2008) 179–86. https://doi.org/10.1038/nmat2133.
[13] R. Vincent, S. Klyatskaya, M. Ruben, W. Wernsdorfer, F. Balestro, Electronic read-out of a single nuclear spin using a molecular spin transistor, Nature. 488 (2012) 357–360. https://doi.org/10.1038/nature11341.
[14] C. Wäckerlin, F. Donati, A. Singha, R. Baltic, S. Rusponi, K. Diller, F. Patthey, M. Pivetta, Y. Lan, S. Klyatskaya, H. Brune, J. Dreiser, Giant Hysteresis of Single-Molecule Magnets Adsorbed on a Nonmagnetic Insulator, Adv. Mater. 28 (2016) 5195–5199. https://doi.org/10.1002/adma.201506305.
[15] N. Ishikawa, M. Sugita, T. Ishikawa, S.-Y. Koshihara, Y. Kaizu, Lanthanide double-decker complexes functioning as magnets at the single-molecular level., J. Am. Chem. Soc. 125 (2003) 8694–5. https://doi.org/10.1021/ja029629n.
[16] N. Ishikawa, M. Sugita, T. Ishikawa, S. Koshihara, Mononuclear Lanthanide Complexes with a Long Magnetization Relaxation Time at High Temperatures : A New Category of Magnets at the Single-Molecular Level, 14 (2004) 1–7.
[17] M. Mannini, F. Bertani, C. Tudisco, L. Malavolti, L. Poggini, K. Misztal, D. Menozzi, A. Motta, E. Otero, P. Ohresser, P. Sainctavit, G.G. Condorelli, E. Dalcanale, R. Sessoli, Magnetic behaviour of $TbPc_2$ single-molecule magnets chemically grafted on silicon surface, Nat. Commun. 5 (2014) 4582. https://doi.org/10.1038/ncomms5582.
[18] M.A. Aldamen, S. Cardona-serra, J.M. Clemente-juan, E. Coronado, A. Gaita-arin, C. Martı, Mononuclear Lanthanide Single Molecule Magnets Based on the (Ln III) Tb , Dy , Ho , Er , Tm , and Yb), 48 (2009) 3467–3479.
[19] C. Ritchie, M. Speldrich, R.W. Gable, L. Sorace, P. Koegerler, C. Boskovic, Utilizing the Adaptive Polyoxometalate $[As_2W_{19}O_{67}(H_2O)]^{14-}$ To Support a Polynuclear Lanthanoid-Based

Single-Molecule Magnet, Inorg. Chem. 50 (2011) 7004–7014. https://doi.org/10.1021/ic200366a.
[20] M. Shiddiq, D. Komijani, Y. Duan, A. Gaita-Ariño, E. Coronado, S. Hill, Enhancing coherence in molecular spin qubits via atomic clock transitions, Nature. 531 (2016) 348–351. https://doi.org/10.1038/nature16984.
[21] K. Liu, W. Shi, P. Cheng, Toward heterometallic single-molecule magnets: Synthetic strategy, structures and properties of 3d–4f discrete complexes, Coord. Chem. Rev. 289–290 (2015) 74–122. https://doi.org/10.1016/J.CCR.2014.10.004.
[22] G. Aromí, D. Aguilà, P. Gamez, F. Luis, O. Roubeau, Design of magnetic coordination complexes for quantum computing., Chem. Soc. Rev. 41 (2012) 537–46. https://doi.org/10.1039/c1cs15115k.
[23] A. Amjad, A.M. Madalan, M. Andruh, A. Caneschi, L. Sorace, Slow Relaxation of Magnetization in an Isostructural Series of Zinc-Lanthanide Complexes: An Integrated EPR and AC Susceptibility Study, Chem. Eur. J. 22 (2016) 12849–12858. https://doi.org/10.1002/chem.201601996.
[24] B.H. Ward, I.B. Rutel, J.S. Brooks, N.S.U. V, J.A. Schlueter, R.W. Winter, G.L. Gard, Millimeter-Wave Spectroscopy of the Organic Spin - Peierls System ′ - (ET) 2 SF 5 CF 2 SO 3, 4 (2001) 1750–1755.
[25] A. Yamashita, A. Watanabe, S. Akine, T. Nabeshima, M. Nakano, T. Yamamura, T. Kajiwara, Wheel-Shaped ErIIIZnII3 Single-Molecule Magnet: A Macrocyclic Approach to Designing Magnetic Anisotropy, Angew. Chemie Int. Ed. 50 (2011) 4016–4019. https://doi.org/10.1002/ANIE.201008180.
[26] D.-P. Li, T.-W. Wang, C.-H. Li, D.-S. Liu, Y.-Z. Li, X.-Z. You, Single-ion magnets based on mononuclear lanthanide complexes with chiral Schiff base ligands [Ln(FTA)$_3$L] (Ln = Sm, Eu, Gd, Tb and Dy)., Chem. Commun. 46 (2010) 2929–31. https://doi.org/10.1039/b924547b.
[27] S. Demir, I.-R. Jeon, J.R. Long, T.D. Harris, Radical ligand-containing single-molecule magnets, Coord. Chem. Rev. 289–290 (2015) 149–176. https://doi.org/10.1016/j.ccr.2014.10.012.
[28] S.-D. Jiang, B.-W. Wang, H.-L. Sun, Z.-M. Wang, S. Gao, An organometallic single-ion magnet, J. Am. Chem. Soc. 133 (2011) 4730–4733. https://doi.org/10.1021/ja200198v.
[29] C.A.P. Goodwin, F. Ortu, D. Reta, N.F. Chilton, D.P. Mills, Molecular magnetic hysteresis at 60 kelvin in dysprosocenium, Nature. 548 (2017) 439–442. https://doi.org/10.1038/nature23447.
[30] F.S. Guo, B.M. Day, Y.C. Chen, M.L. Tong, A. Mansikkamäki, R.A. Layfield, Magnetic hysteresis up to 80 kelvin in a dysprosium metallocene single-molecule magnet, Science 362 (2018) 1400–1403. https://doi.org/10.1126/science.aav0652.
[31] S.-D. Jiang, B.-W. Wang, G. Su, Z.-M. Wang, S. Gao, A Mononuclear Dysprosium Complex Featuring Single-Molecule-Magnet Behavior, Angew. Chemie Int. Ed. 49 (2010) 7448–7451. https://doi.org/10.1002/ANIE.201004027.
[32] S. Zhang, H. Ke, Q. Shi, J. Zhang, Q. Yang, Q. Wei, G. Xie, W. Wang, D. Yang, S. Chen, Dysprosium(III) complexes with a square-antiprism configuration featuring mononuclear single-molecule magnetic behaviours based on different β-diketonate ligands and auxiliary ligands, Dalton Trans. 45 (2016) 5310–5320. https://doi.org/10.1039/C6DT00219F.
[33] Y. Dong, P. Yan, X. Zou, T. Liu, G. Li, Exploiting single-molecule magnets of β-diketone dysprosium complexes with C3v symmetry: suppression of quantum tunneling of magnetization, J. Mater. Chem. C. 3 (2015) 4407–4415. https://doi.org/10.1039/C5TC00321K.
[34] M. Briganti, F. Santanni, L. Tesi, F. Totti, R. Sessoli, A. Lunghi, A Complete Ab Initio View of Orbach and Raman Spin–Lattice Relaxation in a Dysprosium Coordination Compound, J. Am. Chem. Soc. 143 (2021) 13633–13645. https://doi.org/10.1021/JACS.1C05068.

[35] Ming Kong, Xin Feng, Jing Li, Zhao-Bo Hu, Jia Wang, Xiao-Jiao Song, Zhao-Yang Jing, Yi-Quan Zhang, You Song, Structurally modulated single-ion magnets of mononuclear β-diketone dysprosium(III) complexes, Dalton Trans. 49 (2020) 14931–14940. https://doi.org/10.1039/D0DT02864A.
[36] Gong-Jun Chen, Chun-Yan Gao, Jin-Lei Tian, Jinkui Tang, Wen Gu, Xin Liu, Shi-Ping Yan, Dai-Zheng Liao, Peng Cheng, Coordination-perturbed single-molecule magnet behaviour of mononuclear dysprosium complexes, Dalton Trans. 40 (2011) 5579–5583. https://doi.org/10.1039/C1DT10050E.
[37] Sheng Zhang, Wenjiao Mo, Jiangwei Zhang, Haipeng Wu, Min Li, Xingqiang Lü, Bing Yin, Desuo Yang, Experimental and theoretical interpretation of the magnetic behavior of two Dy(III) single-ion magnets constructed through β-diketonate ligands with different substituent groups (–Cl/–OCH_3), RSC Adv. 8 (2018) 29513–29525. https://doi.org/10.1039/C8RA06240D.
[38] P. Cen, M. Wang, X. Ma, L. Chen, Y.-Q. Zhang, Y. Li, D. Tian, X. Liu, Coordination microenvironment perturbed single-ion magnet behavior in a β-diketone Dy(III) complex, CrystEngComm. 22 (2020) 6856–6863. https://doi.org/10.1039/D0CE00935K.
[39] L. Bogani, C. Sangregorio, R. Sessoli, D. Gatteschi, Molecular engineering for single-chain-magnet behavior in a one-dimensional dysprosium-nitronyl nitroxide compound, Angew. Chemie - Int. Ed. 44 (2005) 5817–21. https://doi.org/10.1002/anie.200500464.
[40] G.-J. Chen, Y.-N. Guo, J.-L. Tian, J. Tang, W. Gu, X. Liu, S.-P. Yan, P. Cheng, D.-Z. Liao, Enhancing Anisotropy Barriers of Dysprosium(III) Single-Ion Magnets, Chem. – A Eur. J. 18 (2012) 2484–2487. https://doi.org/10.1002/CHEM.201103816.
[41] X. Yao, P. Yan, G. An,Y. Li, W. Li, G. Li, Investigation of magneto-structural correlation based on a series of seven-coordinated β-diketone Dy(III) single-ion magnets with C2v and C3v local symmetry, Dalton Trans. 47 (2018) 3976-3984. https://doi:10.1039/C7DT04764A.
[42] L. Armelao, S. Quici, F. Barigelletti, G. Accorsi, G. Bottaro, M. Cavazzini, E. Tondello, Design of luminescent lanthanide complexes: From molecules to highly efficient photo-emitting materials, Coord. Chem. Rev. 254 (2010) 487–505. https://doi.org/10.1016/j.ccr.2009.07.025.
[43] J.C.G. Bünzli, On the design of highly luminescent lanthanide complexes, Coord. Chem. Rev. 293–294 (2015) 19–47. https://doi.org/10.1016/J.CCR.2014.10.013.
[44] S.I. Weissman, Intramolecular energy transfer the fluorescence of complexes of europium, J. Chem. Phys. 10 (1942) 214.
[45] G.A. Crosby, R.E. Whan, R.M. Alire, Intramolecular energy transfer in rare earth chelates. Role of the triplet state, J. Chem. Phys. 34 (1961) 743.
[46] M. Latva, Correlation between the lowest triplet state energy level of the ligand and lanthanide(III) luminescence quantum yield, J. Lumin. 75 (1997) 149.
[47] G.A. Bain, J.F. Berry, Diamagnetic Corrections and Pascal's Constants, J. Chem. Educ. 85 (2008) 532. https://doi.org/10.1021/ed085p532.
[48] MathWorks, Matlab, (2021).
[49] T. F. Coleman. Y. Y. Li, An Interior, Trust Region Approach for Nonlinear Minimization Subject to Bounds, Siam J. Optim. 6 (1996) 418–445.
[50] D. Reta, N.F. Chilton, Uncertainty estimates for magnetic relaxation times and magnetic relaxation parameters, Phys. Chem. Chem. Phys. 21 (2019) 23567–23575. https://doi.org/10.1039/c9cp04301b.
[51] G. Malandrino, R. Lo Nigro, I.L. Fragalà, C. Benelli, Yttrium β-Diketonate Glyme MOCVD Precursors: Effects of the Polyether Length on Stabilities, Mass Transport Properties and Coordination Spheres, Eur. J. Inorg. Chem. 2004 (2004) 500–509. https://doi.org/10.1002/EJIC.200300354.
[52] R.D. Shannon, Revised effective ionic radii and systematic studies of interatomic distances in halides and chalcogenides, Acta Crystallogr. Sect. A. 32 (1976) 751–767.

https://doi.org/10.1107/S0567739476001551.
[53] G. Malandrino, I.L. Fragalà, Lanthanide “second-generation” precursors for MOCVD applications: Effects of the metal ionic radius and polyether length on coordination spheres and mass-transport properties, Coord. Chem. Rev. 250 (2006) 1605–1620. https://doi.org/10.1016/J.CCR.2006.03.017.
[54] G. Malandrino, I.L. Fragalà, S. Aime, W. Dastrù, R. Gobetto, C. Benelli, Synthesis, crystal structure and solid-state dynamics of the $La(hfa)_3 \cdot Me(OCH_2CH_2)_4OMe$ (Hhfa = 1,1,1,5,5,5-hexafluoropentane-2,4-dione) precursor for MOCVD applications, J. Chem. Soc. Dalton Trans. (1998) 1509–1512. https://doi.org/10.1039/A708770E.
[55] G. Malandrino, C. Benelli, F. Castelli, I.L. Fragalà, Synthesis, Characterization, Crystal Structure and Mass Transport Properties of Lanthanum β-Diketonate Glyme Complexes, Volatile Precursors for Metal−Organic Chemical Vapor Deposition Applications, Chem. Mater. 10 (1998) 3434–3444. https://doi.org/10.1021/CM980172J.
[56] I. Cimatti, X. Yi, R. Sessoli, M. Puget, B. Le Guennic, J. Jung, T. Guizouarn, A. Magnani, K. Bernot, M. Mannini, Chemical tailoring of Single Molecule Magnet behavior in films of Dy(III) dimers, Appl. Surf. Sci. 432 (2018) 7–14. https://doi.org/10.1016/J.APSUSC.2017.06.024.
[57] A. Amjad, A. Figuerola, A. Caneschi, L. Sorace, Multiple Magnetization Reversal Channels Observed in a 3d-4f Single Molecule Magnet, Magnetochemistry 2 (2016) 27. https://doi.org/10.3390/magnetochemistry2020027.
[58] E. Rousset, M. Piccardo, M.E. Boulon, R.W. Gable, A. Soncini, L. Sorace, C. Boskovic, Slow Magnetic Relaxation in Lanthanoid Crown Ether Complexes: Interplay of Raman and Anomalous Phonon Bottleneck Processes, Chem. - A Eur. J. 24 (2018) 14768–14785. https://doi.org/10.1002/chem.201802779.
[59] S.T. Liddle, J. Van Slageren, Improving f-element single molecule magnets, Chem. Soc. Rev. 44 (2015) 6655–6669. https://doi.org/10.1039/c5cs00222b.
[60] R. Orbach, Spin-Lattice Relaxation in Rare-Earth Salts : Field Dependence of the Two-Phonon Process, Proc. R. Soc. London. Ser. A Math. Phys. Eng. Sci. 264 (1961) 485–495.
[61] M.A. Guedes, T.B. Paolini, M.C.F.C. Felinto, J. Kai, L.A.O. Nunes, O.L. Malta, H.F. Brito, Synthesis, characterization and spectroscopic investigation of new tetrakis(acetylacetonato)thulate(III) complexes containing alkaline metals as countercations, J. Lumin. 131 (2011) 99–103. https://doi.org/10.1016/J.JLUMIN.2010.09.006.
[62] J. Priya, N.K. Gondia, A.K. Kunti, S.K. Sharma, Pure White Light Emitting Tetrakis β-diketonate Dysprosium Complexes for OLED Applications, ECS J. Solid State Sci. Technol. 5 (2016) R166–R171. https://doi.org/10.1149/2.0101610JSS.